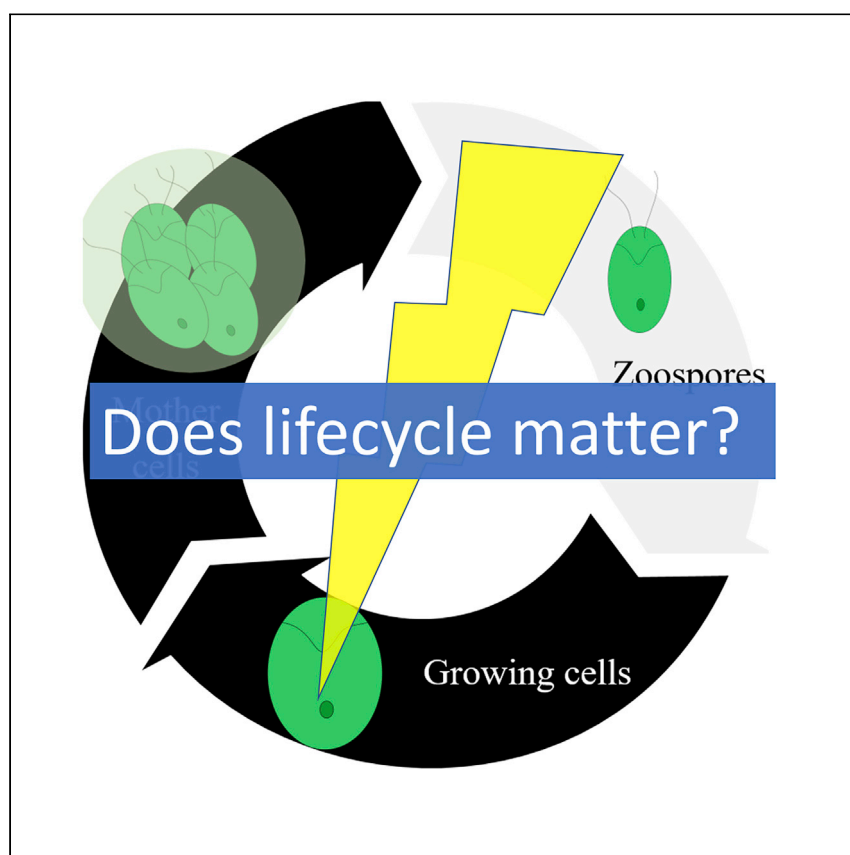


Report

Does the life cycle stage matter for distinguishing phytoplankton via fluoro-electrochemical microscopy?



Here, Yu et al. develop a method for automation to distinguish phytoplankton in the real world without the need to manually identify the life stages of each species, which may co-exist in a natural environment. Using a fluoro-electrochemical analysis, different life stages of phytoplankton are shown to be identical toward electrogenerated oxidative damage with respect to fluorescence switch-off.

Jiahao Yu, Minjun Yang,
Christopher Batchelor-McAuley,
Samuel Barton, Rosalind E.M.
Rickaby, Heather A. Bouman,
Richard G. Compton

richard.compton@chem.ox.ac.uk

Highlights

Three life stages of
Chlamydomonas concordia are
investigated under oxidative
stress

Oxidative susceptibility of
phytoplankton is shown
independent of life stage

Basis for real-world species
analysis via a fluoro-
electrochemical method is
established

Yu et al., Cell Reports Physical Science 4,
101223

January 18, 2023 © 2022 The Authors.

<https://doi.org/10.1016/j.xcrp.2022.101223>



Report

Does the life cycle stage matter for distinguishing phytoplankton via fluoro-electrochemical microscopy?

Jiahao Yu,¹ Minjun Yang,¹ Christopher Batchelor-McAuley,¹ Samuel Barton,² Rosalind E.M. Rickaby,² Heather A. Bouman,² and Richard G. Compton^{1,3,*}

SUMMARY

Phytoplankton have species-specific responses toward electrogenerated oxidants, allowing high-throughput species analysis. Herein, a fluoro-electrochemical method is used to expose single *Chlamydomonas concordia* vegetative cells at different points within their life cycle to electro-generated oxidants from seawater. The resulting decay in fluorescence from chlorophyll-a is measured as a function of time and drops to zero for phytoplankton adjacent to the electrode over a period of a few seconds. The chlorophyll-a transient timescale allows mother cells, which are distinctively larger and require a larger quantity of oxidants, to be distinguished from either zoospores or “growing” cells, while all the cells show the same intrinsic susceptibility modulated only by the size of the phytoplankton. These observations are essential for the future automated characterization of the speciation of phytoplankton populations as they show that there is no need to manually identify the life cycle stage.

INTRODUCTION

Marine phytoplankton are the Earth's powerhouse owing to first their contribution of more than 50% of the Earth's O₂ production and second their ability to sequester CO₂ from the atmosphere at a rate that is comparable to that released by humans (>10¹⁵ g year⁻¹). Natural communities of phytoplankton are incredibly diverse¹ and are comprised of different phytoplankton function groups, for example pico-autotrophs, calcifiers, and silicifiers, that vary greatly in their biogeochemical functions.² Moreover, multiple life stages of phytoplankton, which are species specific, have been reported within the population of a species.¹ However, due to the difficulties of observing the often rapid transitions among them in the natural environment, and in any case not being immediately obvious for some species,³ the functioning of life cycles in phytoplankton ecology and evolution are not well reported⁴ despite such data being vital to models of ocean health and biogeochemical composition.

A systematic and high-throughput identification of different species of phytoplankton and their respective life stages are therefore important for ecological studies, but only limited methods are available for this task.⁴ Flow cytometry⁵ is a high-throughput approach used to screen and separate different phytoplankton groups with a distinctive difference in their light scattering and/or autofluorescence properties. For most eukaryotic phytoplankton cells, however, owing to similar red chlorophyll autofluorescence, the flow cytometer is limited to categorizing species with a notable size differences into either “small” or “large” phytoplankton.⁶ Identification of the life stages of phytoplankton, which are usually not too different in

¹Physical and Theoretical Chemistry Laboratory, Department of Chemistry, University of Oxford, South Parks Road, Oxford, UK

²Department of Earth Sciences, University of Oxford, South Parks Road, Oxford, UK

³Lead contact

*Correspondence: richard.compton@chem.ox.ac.uk
<https://doi.org/10.1016/j.xcrp.2022.101223>



cellular size aside from the time-consuming and costly DNA staining,⁷ otherwise requires a trained operator microscopically examining matching cellular traits and features such as morphology differences, mobility, sexual behavior. etc.¹

Driven by the need to advance techniques in rapidly quantifying changes in phytoplankton community structure in response to environmental change, recent proof-of-concept electrochemical work has revealed that different species of phytoplankton (representing different functional groups) have different and analytically useful responses toward oxidants electro-generated from and in seawater. This was revealed by their rate of decay of chlorophyll-a (chl-a) fluorescence over tens of seconds of the experiment when exposed to the oxidants generated by the application of a potential or current on an electrode within the seawater medium.^{8,9} This observation may provide a complementary approach to the flow cytometer as a mean to separate different species or functional types of phytoplankton irrespective of their size. This approach has great promise as the basis for a rapid throughput detection technique for different phytoplankton functional types, including for ship-board and autonomous measurements, not least since the previous work⁸ showed that the electrochemically stimulated decay of chl-a fluorescence permitted differentiation in the relative susceptibility of 6 different phytoplankton species. However, those measurements were made without regard for the point of the life cycle of the phytoplankton. It is thus essential to identify any intraspecies life cycle dependency of the fluorescence transients to facilitate the development of automated *in situ* interspecies differentiation using the above-described fluoro-electrochemical technique in place of bench-top microscopic analysis.

In this work, we investigate the chl-a response of different life stages of the marine green algae *Chlamydomonas concordia* toward electrogenerated oxidants. A constant current is applied to a glassy carbon electrode, which acts as both a supporting substrate for the algae cells and an electrochemical generator, to generate millimolar oxidants at the electrode interface. The mass transport, electrode kinetics, and redox chemistry are well established.⁹ Optical images provide the chl-a response of individual *C. concordia* cells in fluoro-electrochemical experiments to allow their susceptibility toward electro-generated oxidants to be investigated on a single-entity basis and as a function of the different stages of the life cycle of the algae. In the following, we first use the life forms of the *Chlamydomonas* genus reported in the literature to develop a clear protocol for categorizing each based on optical microscopy. We then apply fluoro-electrochemical experiments to investigate the effect of electrochemically induced oxidative stress on different life stages of *C. concordia* cells. In particular, three types of *C. concordia* vegetative cells, more of which are described below, were studied—zoospores, growing, and mother cells—with the fluorescent response shown to be independent of life stage and so encouraging the use of fluoro-electrochemical microscopy for automated phytoplankton identification. The work herein is essential to real-world sensing using fluoro-electrochemical techniques as different life stages may appear in real-world samples.

RESULTS AND DISCUSSION

Life cycles of *Chlamydomonas*

The life cycle of freshwater *Chlamydomonas* is varied and complex; schematics can be found in the literature and are shown in Figure S1.^{10,11} In short, in the vegetative life cycle of *Chlamydomonas* cells, apparent cytokinesis results in the “liberation” of biflagellated daughter cells (zoospores). The flagellated cells grow during the light phase, which is the part of the photoperiod when the cells are exposed to light. Toward the end of the light phase (“day”), the zoospore cell deflagellates to initiate tubulin production¹² and develops into a “mother” cell in the dark phase (“night”),

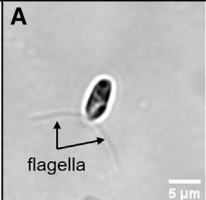
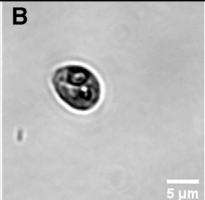
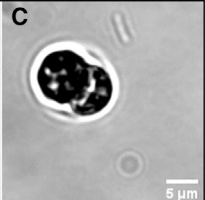
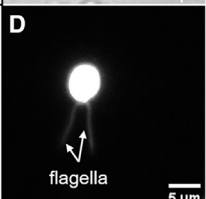
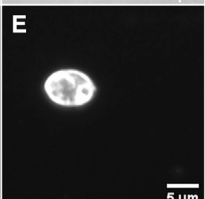
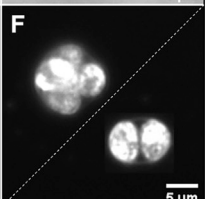
	Type 1 Zoospore (n=67)	Type 2 Growing cell (n=14)	Type 3 Mature cell (n=31)
Bright-field image			
Dark-field image			
Mobility observed	Yes	No	No
Avg. length/width ratio	1.45 ± 0.22	1.17 ± 0.10	1.14 ± 0.10
Cell division observed	No	No	Mostly Yes
Effective Diameter (μm)	6.65 ± 0.71	6.53 ± 0.37	8.58 ± 0.82

Figure 1. Optical images of three types of morphology distinct cells were observed in the *C. concordia* culture (types 1, 2, and 3)

Images (A–C) were obtained under bright-field illumination and (D–F) using a dark-field condenser. The arrows in (A) and (D) point to flagella. Mobility indicates cellular movements usually unidirectional at speed ($>10 \mu\text{m/s}$) more than 10 times that expected for Brownian motion. Length is the measurement of the longest cellular dimension excluding flagella, and the width is the perpendicular cellular dimension at half-length. Cell division is the observation of more than one distinct cell present inside the cell membrane. The effective diameter is the diameter of a perfect circle with its area equal to the projection area of the phytoplankton cell. Scale bars: $5 \mu\text{m}$.

where between two and four daughter cells are formed. The life cycle repeats at the first sight of “dawn.” The vegetative cycle may continue indefinitely provided that sufficient CO_2 , light, and nutrients are present. In the event of nitrogen depletion, however, *Chlamydomonas* transits from the vegetative (asexual) to a “sexual” phase, where gametes of the opposite sex mate to form a quadriflagellate zygote before it undergoes meiotic divisions to release either four or eight vegetative cells.¹⁰ It is worth noting that most of the available literature on the life stages of *Chlamydomonas* is on *Chlamydomonas reinhardtii* (a fresh water species), and therefore without further knowledge, we might assume that marine species of the *Chlamydomonas* genus show the same asexual and sexual life stages.

In this work, a marine *C. concordia* culture (Roscoff Culture Collection [RCC1], France) was first imaged and characterized under optical microscopy using a $40\times$ objective lens and under bright-field (Figures 1A–1C) and dark-field illuminations (Figures 1D–1F). A variety of cells were seen, and three were categorized identified based on size, shape, and the presence or absence of flagella. A short video showing the three cell types is attached separately online in the supplemental information and a snapshot image of the video is provided in Figure S2. Figure 1 shows optical images of the three morphologically distinctive types of cells observed in a population of *C. concordia* culture.¹³ The type 1 cells are ovoid and biflagellated cells with the length of the flagella longer than the body. Type 1 cells are mobile and often seen to travel unidirectionally at speeds in excess of $10 \mu\text{m s}^{-1}$ (see Video S1), which is much faster than that expected as a result of Brownian motion, where the root-mean-square distance of a $10\text{-}\mu\text{m}$ -sized spherical particle diffused in 1 s is estimated to be $0.3 \mu\text{m}$. Type 2 cells are ovoid to near spherical

in shape, are not mobile, and lack flagella. Type 3 cells are larger than types 1 and 2 and are immobile and spherical cells. Both type 2 and 3 cells, if deposited on a surface, remain stationary on the substrate over a timescale of minutes. Two or four daughter cells are often visible within the circular membrane of type 3 cells, which indicates mitosis (see Figure 1F). In terms of shape and size, type 1 cells are smaller than type 2 or 3 with a length-to-width ratio of 1.5 ± 0.2 (see Figure S3). Types 2 and 3 are more spherical compared with type 1, with an averaged observed length-to-width ratio of 1.1 ± 0.1 . Type 3 cells have an effective diameter $\approx 8.5 \mu\text{m}$, which is distinctively larger than type 1 or 2 cells (effective diameters $\approx 6.5 \mu\text{m}$) where the effective diameter was calculated using the projection area of the planktonic cell assuming a perfect circle, as summarized in Figures S5 and S6. The characteristics of the three types of cell are summarized in Figure 1.

It can be deduced from the above-mentioned cell observations, compared with the literature observations for the *Chlamydomonas* genus,^{10,11} that the population of the marine species *C. concordia* is in the vegetative life cycle. Specifically, only biflagellated cells (zoospores) were seen, with no signs of quadriflagellate cells (zygote). Moreover, that a maximum of four daughter cells were seen for mother cells undergoing mitosis is an indication of the vegetative life cycle, in contrast to a maximum of eight daughter cells in the sexual stage. These observations contrast with the other life cycles, namely gametic and zygotic, which are characterized by quadriflagellate cells undergoing meiotic division to yield four to eight haploid vegetative cells. Within our suggested classification, type 1 cells are zoospores, type 3 are mother cells showing signs of mitosis, and type 2 are deflagellated zoospores in between types 1 and 3 within the life cycle, termed herein as growing cells. To distinguish the three types of cells in the fluoro-electrochemical experiment, a flow chart (shown in Figure S4) was used systematically as a separation protocol based on the cell mobility, length-to-width ratio, and the effective diameter of individual cells. An additional category, type 4, is introduced for the inclusivity of non-mobile cells that are not fully or unambiguously characterizable as type 2 or 3. This indeterminacy was observed in 7% of the cells examined and is expected as the vegetative life cycle (cytokinesis, deflagellation, cellular growth, and mitosis division) occurs continuously and not via stepwise processes.

Life stage response to electrogenerated oxidants

Figure 2 shows the average chl-a fluorescence intensity of the different *C. concordia* cell types in the vegetative life cycle as a function of time following the switch on of the electrogeneration of oxidants during the fluoro-electrochemical experiment. The *C. concordia* cells were dropcasted onto the surface of a glassy carbon electrode at a density of approximately 500 cells per mm^2 . The electrode acts as both a physical support and as an electrode for generating the oxidants. A schematic depicting the fluoro-electrochemical experiment is given in the supplemental information.^{9,14} The *C. concordia* cells were immersed in artificial seawater based culture medium (see supplemental experimental procedures) and were exposed to continuous fluorescence excitation starting 40 s before a step change in the applied current from 0 A to 50 μA . In previous work,⁹ we showed that the step change in the applied current results in concomitant electro-oxidation of Br^- , Cl^- , and H_2O present at different concentrations in seawater. The electro-generated oxidants diffuse from the interface and react destructively with the cells, differentially switching off the chl-a fluorescence of various species of phytoplankton using electrochemistry.^{8,9} For all four types of *C. concordia* vegetative cells, catastrophic drops in the chl-a fluorescence intensity were seen after ~ 2 s of the current step. The chl-a transients of type 1 and 2 cells are very similar and are undistinguishable from each other, while type 3, the mother cells, require a distinctively longer time for their chl-a to be

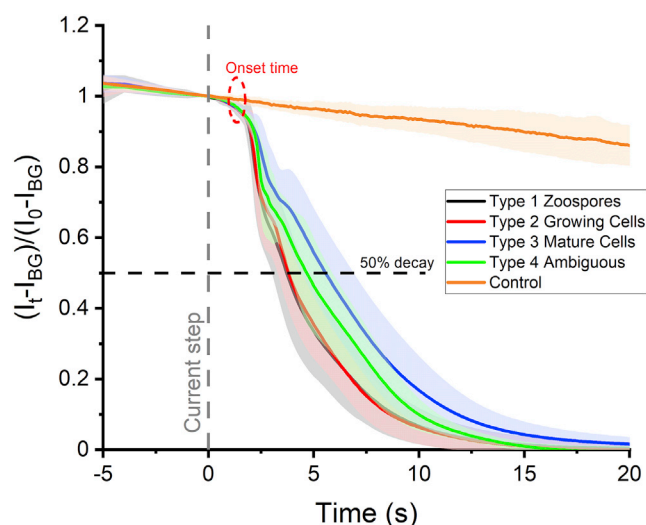


Figure 2. The average fluorescence intensity of the four types of *C. concordia* cells as a function of time during the fluoro-electrochemical experiment

For $t < 0$ s, a constant current of 0 A was applied to the working electrode for 40 s. At $t = 0$ s, the applied current is stepped to 50 μ A and maintained at this value throughout the experiment. The chl-*a* fluorescence intensity ($\lambda_{\text{ex}} = 475 \pm 25$ nm, $\lambda_{\text{em}} > 590$ nm) was continuously monitored during the entire experiment. The orange line describes a control experiment in which the fluoro-electrochemical cell was disconnected from the potentiostat during the course of the experiment. F/2 culture medium was used as electrolyte (see supplemental information). The transients were averaged over four technical replicates. Sample size: type 1, $n = 67$; type 2, $n = 14$; type 3, $n = 31$; type 4, $n = 8$. The shaded region of each line plot represents the standard deviations.

switched off. The average transient of the cells that cannot be confidently identified as either type 2 or 3 (labeled type 4, ambiguous cells) reflects the average transient of type 2 and 3 cells. In the absence of any electrogenerated oxidative stress (Figure 2 orange line), the fluorescence transient of phytoplankton cells was negligibly affected over the timescale of the experiment.

To investigate the factors resulting in the different behaviors toward oxidative damage, the total numbers of moles of oxidant generated that could have reacted with the individual cells under mass transport control from the electrode to the cell was calculated using the following expression derived from the Sand equation^{15,16} (derivation of Equation 1 can be found in previous work⁹):

$$\text{mol of oxidants} = \frac{\ln(2)16\pi^{1/2}D_{\text{Ox}}^{1/2}r_{\text{sphere}}it^{3/2}}{3nFA}, \quad (\text{Equation 1})$$

where D_{Ox} is the diffusion coefficient of the oxidants and is assumed to take a value of $\sim 1 \times 10^{-9}$ $\text{m}^2 \text{s}^{-1}$; r_{sphere} is the approximate radius of the phytoplankton cell (m) assumed to be spherical; i is the constant applied current (A); n is the number of electrons transferred per molecular oxidative event; F is the Faraday constant (96,485.3 s A mol^{-1}); A is the geometric area of the electrode (m^2); and t , as will be discussed below, is either the time at which the quickest drop in the intensity was seen or the time required for the fluorescence intensity to drop below 50%. These two characteristic times are depicted on Figure 2 for illustration purposes. These two calculation methods allow different parts of the *C. concordia* chl-*a* transients to be analyzed on a single-cell basis with the aim to provide kinetic insights into the fluorescence quenching processes as induced by electro-generated oxidants in the fluoro-electrochemical experiments.

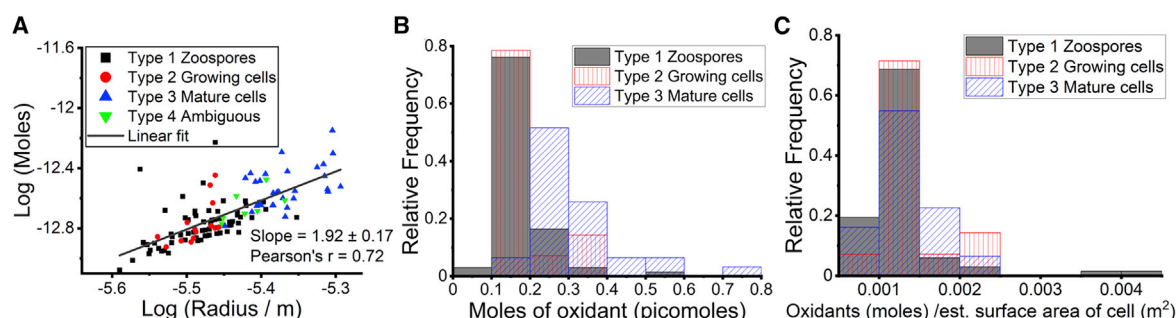


Figure 3. The number of oxidants required to cause a catastrophic drop in the chl-a fluorescence intensity of various types of *C. concordia* cells plotted against the cellular radius

At $t = 0$, the applied current is stepped from 0 A to 50 μ A.

(A) The calculated number of moles of oxidants. The slope of the linear line of best fit was obtained by fitting data across all cell types, and the error is the SE of the slope.

(B) Distribution of the number of moles of oxidants required to cause a catastrophic drop in the chl-a fluorescence intensity of various types of *C. concordia* cells.

(C) The number of moles of oxidant required normalized against cellular area. The cell area was estimated from the cellular projection area assuming a perfect sphere. The sample size of each of the cell types is stated in the Figure 2 legend.

Chlorophyll transient characteristics: Catastrophic drop and 50% switch off

First, we investigate the part of chl-a transients where a catastrophic drop in the intensity was seen. In Figure 2, this is at $\sim t = 2$ s. The time until the catastrophic drop, as defined by the time until the quickest change in the intensity gradient, was analyzed systematically on a per-cell basis using the second derivative of intensity with respect to time leading to an estimate of the time required to estimate the initiation of the drop.⁸ Figure 3A shows the calculated number of moles of oxidant that have reacted in the period of time before the catastrophic drop in chl-a fluorescence intensity plotted against the radius of each individual cell. Note the logarithmic scale. The slope of the log-log plot is 1.92 ± 0.17 , which suggests, interestingly, that the number of moles of oxidant required to initiate the catastrophic drop in chl-a fluorescence intensity of the phytoplankton cell is related to its surface area (proportional to radius squared). This is further shown in Figures 3B and 3C by the overlap of histograms once the moles of oxidant were normalized against the surface area of the individual cells. This again suggests that the initiation of the chl-a switch off is related to the area of the cell wall since the latter scales with r^2 . Sub-picomole oxidants were required to initiate the onset of chl-a switch off, as can be seen in Figure 3B. Next, we investigate later in the chl-a transient, after the phytoplankton cell wall is inferred to have been compromised/breached by the electro-generated oxidants. The time taken for 50% of the chl-a fluorescence intensity to be oxidatively quenched on a single-cell basis was extracted from the transient shown in Figure 2. This time, t , was used in combination with Equation 1 to give the number of moles of oxidant that have reacted under a mass transport control to result in a 50% switch off of the fluorescence intensity of individual cells. Figure 4A plots the calculated moles of oxidant required to switch off 50% of the fluorescence intensity against the radius of the phytoplankton cell, plotted on a logarithmic scale. A strong cubic correlation with log-log slope of 2.92 ± 0.18 can be seen between the cellular radius and the total moles of oxidant reacted. Figures 4B and 4C show the histograms plotted separately for the different type of cells. The average number of moles of oxidant required to switch off 50% of the chl-a is $0.41 (\pm 0.17)$ picomoles for type 1, $0.40 (\pm 0.12)$ picomoles for type 2, and $0.92 (\pm 0.32)$ picomoles for type 3. An overlap in the histogram distribution can be seen after normalizing the moles of oxidant against the volume of the individual phytoplankton cell. It is evident that both methods of analysis, either at

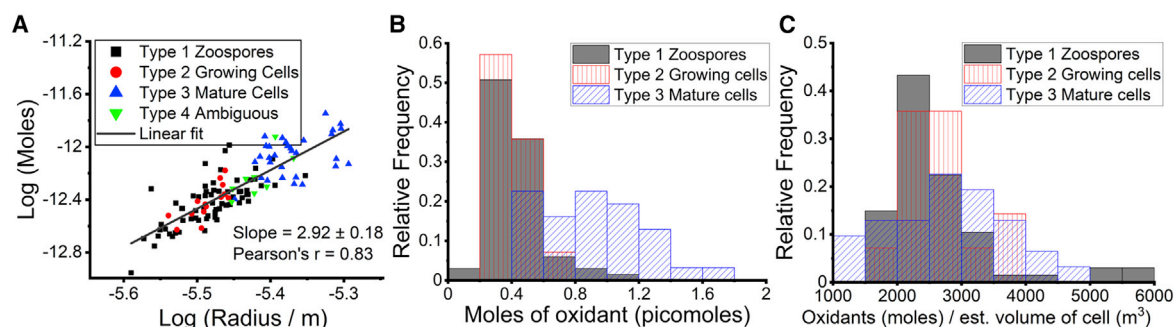


Figure 4. The number of moles of oxidant required to switch off 50% chl-a fluorescence intensity of various types of *C. concordia* cells plotted against the cellular radius as a log-log plot

At $t = 0$, the applied current is stepped from 0 A to 50 μA .

(A) The calculated number of moles of oxidant. The slope of the linear line of best fit was obtained by fitting data across all cell types, and the error is the SE of the slope.

(B) Distribution of the number of moles of oxidant required to switch off 50% fluorescence intensity of various types of *C. concordia* cells.

(C) Distribution of the number of moles of oxidant required for the 50% switch off normalized against cellular volume. Cell volumes were estimated from the cellular projection area assuming a perfect sphere. The sample size of each of the cell types is stated in the Figure 2 legend.

the onset of the switch off or at the point of 50% of its original intensity, indicate that type 3 cells require distinctively more oxidants than either type 1 and 2, thus providing a basis for a distinction to be made and so permitting the mother cells to be identified from the others on this basis. Shown in Figure S7 is the integrated raw intensity of the individual phytoplankton cell versus their cellular radius. The slope in the logarithmic scale is 2.8 ± 0.3 , indicating that the amount of chl-a content to be quenched is proportional to the volume of the *C. concordia* cells. Shown in Figure S8 is the integrated raw intensity of the individual phytoplankton cell versus the time required for 50% of their fluorescence to be switched off by electrochemical generated oxidants. A log-log slope of $1.2 (\pm 0.2)$ is seen from Figure S8, and this is consistent with Sand's equation (Equation 1 in the main text), where the total amount of moles of oxidant delivered to each individual cell is proportional to time raised to the power of 1.5.

Interestingly, shown in Figure S9, the log-log slope analyzed using the characteristic time between the 50% decay time and the first onset time of rapid decay is 3.7 ± 0.2 . The value of this slope is higher than that calculated from the start of the experiment to the 50% decay time (slope of 2.9 ± 0.2). This is likely because the phytoplankton cell, in its simplest terms and within the context of this experiment, can be viewed as a sack of chl-a surrounded by a protective layer to be breached by electrogenerated radicals. Due to the small size of the plankton cell ($\sim 2\text{--}10 \mu\text{m}$) relative to the diffusional distance of the electrogenerated species in the timescale of the experiment ($\sim 10 \text{ s}$), the phytoplankton cell can be simply modeled as a homogeneous bath of chemicals with a protective membrane.¹⁷ To initiate the initial decay of the chl-a signal, a partial breach or penetration of the protective layer has to occur before a measurable loss in the chl-a signal is seen. To titrate away 50% of the chl-a signal, however, more oxidants are required, as can be seen in Figure 2 by its characteristic time compared with that required to initiate the onset of chl-a decay. Since the cell is "bathed" by oxidants, and since oxidants are highly reactive with a short lifetime, it is not unreasonable to conclude that oxidants react with the remainder of the projective layer as well as chl-a leading up to the 50% decay. This is consistent with the experimental observation that the amounts of oxidants required to initiate the onset of the chl-a switch off are proportional to cellular radius squared (cell wall $\propto r^2$), while the amount required to bring about the

“titration” of the chl-a contents to 50% of the original intensity from the onset of electrolysis is proportional to the cellular radius cubed (volume $\propto r^3$).

The results reported herein provide an essential basis for real-world automated sampling. By measuring the fluorescent decay kinetics of individual cells, as demonstrated in this work, the total number of moles of oxidant required to be delivered for their chl-a signal to switch off reveals the speciation of the phytoplankton in a mixed solution regardless of its life stage. This gives the physical basis for prototype automated devices to be designed for high-throughput field measurements with field results compared with a pre-determined phytoplankton “susceptibility” library and avoids the need for bench-top microscopic analysis.

To conclude, this work reveals that different life stages within the population of one single species of phytoplankton, *C. concordia*, i.e., different cell types (zoospores, growing, and mature cells), are biologically equivalent toward oxidative stress after size normalization. The amounts of oxidants required to trigger the onset of switch off and to 50% of chl-a fluorescence intensity is proportional to the cellular radius squared and cubed, respectively. This is suggestive that the transport of oxidants across the planktonic cell wall ($\propto r^2$), either reacting chemically or simply as mass transport across the barrier, is the rate-determining step before the onset of the chl-a switch off. The number of oxidants required to “titrate” the chl-a content is proportional to the cellular volume ($\propto r^3$). This offers an essential basis for the automation of phytoplankton function group identification in the real world without the need to identify the life stages of each species since several life stages of one species may co-exist in the natural environment.

EXPERIMENTAL PROCEDURES

Resource availability

Lead contact

Further information and requests for resources and reagents should be directed to and will be fulfilled by the lead contact, Prof. Dr. Richard G. Compton (richard.compton@chem.ox.ac.uk).

Materials availability

This study did not generate new, unique reagents.

Data and code availability

This paper does not report original code. The data supporting the current study are available from the [lead contact](#) upon reasonable request.

Chemicals

All chemicals were supplied by Sigma-Aldrich. All chemicals were of analytical standard and applied without further purification. Ultrapure water (Millipore, resistivity 18.2 M Ω cm at 25°C) was utilized to make synthetic ocean water.

Phytoplankton cultures

C. concordia (marine green alga, RCC1) strain was supplied by the RCC, France. Stock culture of RCC1 underwent regular sub-culturing into fresh growth medium under sterile conditions during the exponential growth phase. The growth medium consists of an Aquil¹⁸ synthetic ocean water with F/2 enrichments.^{19,20} The culture was kept under a 14:10 h light-dark cycle with a light intensity of 20–40 $\mu\text{mol m}^{-2} \text{s}^{-1}$ at 17°C in a PHCbi MLR-352-PE Incubator (PHC Europe B.V.).

3D-printed cell setup and image analysis

The fluoro-electrochemical cell was designed digitally in Fusion 360 (Autodesk) and was subsequently printed using a Form2 3D printer equipped with white resin (Formlabs, Somerville, MA, USA). A schematic of the opto-electrochemical cell showing the three-electrode setup is reported elsewhere.¹⁴ The 3D-printed opto-electrochemical cell¹⁴ (dimensions = 7 × 3 × 1 cm) hosts a reference electrode (RE-2BP, saturated calomel electrode [SCE], ALS, Tokyo, Japan), a graphite counter rod, and a glassy carbon working electrode (3 mm diameter, MF-2012, BASi, West Lafayette, IN, USA). The working electrode was inserted bottom up into the opto-electrochemical cell with the surface of the electrode facing the objective lens (20×, numerical aperture [NA] = 0.5, EC Plan-Neofluar, Carl Zeiss, Cambridge U.K) of a conventional upright microscope (Zeiss A1 Axio Examiner, Carl Zeiss). The surface of the working electrode acts as both a supporting substrate and an electrochemical generator for the phytoplankton. Dark-field images were taken under a 40× oil-immersion objective lens (plan-apochromat, Carl Zeiss) using an oil-immersion dark-field condenser (NA = 1.2/1.4, Carl Zeiss). Fluorescence images of the phytoplankton cell were acquired using an excitation filter from Thorlab (fluorescein isothiocyanate [FITC] 475 ± 35 nm); the dichromic mirror and emission filter were from Zeiss Filter Set 15, which transmits emission wavelengths above 590 nm. The fluorescence excitation light source was provided by an LQ-HXP 120 V lamp. The projected areas of the phytoplankton were measured using ImageJ free-ware (Fiji distribution). The effective diameters of the phytoplankton cells were calculated assuming a perfect circle ($\text{Area} = \pi(\frac{d}{2})^2$). Galvanostatic control, microscopy setup, and image analysis were described in detail in authors' previous work.^{9,14}

SUPPLEMENTAL INFORMATION

Supplemental information can be found online at <https://doi.org/10.1016/j.xcrp.2022.101223>.

ACKNOWLEDGMENTS

This work was carried out with the support of the Oxford Martin School Program on Monitoring Ocean Ecosystems.

AUTHOR CONTRIBUTIONS

Conceptualization, J.Y., M.Y., C.B.-M., and R.G.C.; experiment, J.Y. (lead) and S.B. (culture); methodology, M.Y. and C.B.-M.; software, M.Y. and C.B.-M.; formal analysis, J.Y.; visualization, M.Y. and C.B.-M.; supervision, R.G.C.; writing – original draft, J.Y. and M.Y.; writing – review & editing, M.Y., C.B.-M., S.B., R.G.C., R.E.M.R., and H.A.B.

DECLARATION OF INTERESTS

The authors declare no competing interests.

INCLUSION AND DIVERSITY

One or more of the authors of this paper self-identifies as an underrepresented ethnic minority in their field of research or within their geographical location.

Received: October 6, 2022

Revised: November 17, 2022

Accepted: December 14, 2022

Published: January 11, 2023

REFERENCES

1. Tomas, C.R. (1997). *Identifying Marine Phytoplankton* (Elsevier).
2. Nair, A., Sathyendranath, S., Platt, T., Morales, J., Stuart, V., Forget, M.-H., Devred, E., and Bouman, H. (2008). Remote sensing of phytoplankton functional types. *Remote Sens. Environ.* 112, 3366–3375. <https://doi.org/10.1016/j.rse.2008.01.021>.
3. Huo, S., Li, X., Xi, B., Zhang, H., Ma, C., and He, Z. (2020). Combining morphological and metabarcoding approaches reveals the freshwater eukaryotic phytoplankton community. *Environ. Sci. Eur.* 32, 37. <https://doi.org/10.1186/s12302-020-00321-w>.
4. Von Dassow, P., and Montresor, M. (2011). Unveiling the mysteries of phytoplankton life cycles: patterns and opportunities behind complexity. *J. Plankton Res.* 33, 3–12. <https://doi.org/10.1093/plankt/fbq137>.
5. Dunker, S., Boho, D., Wäldchen, J., and Mäder, P. (2018). Combining high-throughput imaging flow cytometry and deep learning for efficient species and life-cycle stage identification of phytoplankton. *BMC Ecol.* 18, 51. <https://doi.org/10.1186/s12898-018-0209-5>.
6. Collier, J.L. (2000). Flow cytometry and the single cell in phycology. *J. Phycol.* 36, 628–644. <https://doi.org/10.1046/j.1529-8817.2000.99215.x>.
7. Jacquet, S., Partensky, F., Marie, D., Casotti, R., and Vaulot, D. (2001). Cell cycle regulation by light in *Prochlorococcus* strains. *Appl. Environ. Microbiol.* 67, 782–790. <https://doi.org/10.1128/AEM.67.2.782-790.2001>.
8. Yang, M., Batchelor-McAuley, C., Chen, L., Guo, Y., Zhang, Q., Rickaby, R.E.M., Bouman, H.A., and Compton, R.G. (2019). Fluoro-electrochemical microscopy reveals group specific differential susceptibility of phytoplankton towards oxidative damage. *Chem. Sci.* 10, 7988–7993. <https://doi.org/10.1039/C9SC02699A>.
9. Yu, J., Yang, M., Batchelor-McAuley, C., Barton, S., Rickaby, R.E.M., Bouman, H.A., and Compton, R.G. (2022). Rapid optoelectrochemical differentiation of marine phytoplankton. *ACS Meas. Sci.* 2, 342–350. <https://doi.org/10.1021/acsmeasuresciau.2c00017>.
10. Weeks, D.P., and Collis, P.S. (1979). Induction and synthesis of tubulin during the cell cycle and life cycle of *Chlamydomonas reinhardtii*. *Dev. Biol.* 69, 400–407. [https://doi.org/10.1016/0012-1606\(79\)90300-2](https://doi.org/10.1016/0012-1606(79)90300-2).
11. Mihara, S., and HASE, E. (1971). Studies on the vegetative life cycle of *Chlamydomonas reinhardtii* Dangeard in synchronous culture I. Some characteristics of the cell cycle. *Plant Cell Physiol.* 12, 225–236. <https://doi.org/10.1093/oxfordjournals.pcp.a074616>.
12. Weeks, D.P., and Collis, P.S. (1976). Induction of microtubule protein synthesis in *Chlamydomonas reinhardtii* during flagellar regeneration. *Cell* 9, 15–27. [https://doi.org/10.1016/0092-8674\(76\)90048-9](https://doi.org/10.1016/0092-8674(76)90048-9).
13. Roscoff Culture Collection. <https://roscoff-culture-collection.org/rcc-strain-details/1>.
14. Yang, M., Batchelor-McAuley, C., Barton, S., Rickaby, R.E.M., Bouman, H.A., and Compton, R.G. (2022). Single-entity coccolithophore electrochemistry shows size is no guide to the degree of calcification. *Environ. Sci. Adv.* 1, 156–163. <https://doi.org/10.1039/D2VA00025C>.
15. Bard, A.J., and Faulkner, L.R. (2000). *Electrochemical Methods: Fundamentals and Applications*, 2nd Edition (John Wiley & Sons).
16. Sand, H.J. (1901). III. On the concentration at the electrodes in a solution, with special reference to the liberation of hydrogen by electrolysis of a mixture of copper sulphate and sulphuric acid. *Lond. Edinb. Dublin Philos. Mag. J. Sci.* 1, 45–79. <https://doi.org/10.1080/14786440109462590>.
17. Sasso, S., Stibor, H., Mittag, M., and Grossman, A.R. (2018). The Natural History of Model Organisms: from molecular manipulation of domesticated *Chlamydomonas reinhardtii* to survival in nature. *Elife* 7, e39233. <https://doi.org/10.7554/eLife.39233>.
18. Morel, F.M.M., Rueter, J.G., Anderson, D.M., and Guillard, R.R.L. (1979). Aquil: a chemically defined phytoplankton culture medium for trace metal studies. *J. Phycol.* 15, 135–141. <https://doi.org/10.1111/j.1529-8817.1979.tb02976.x>.
19. Guillard, R.R. (1975). Culture of phytoplankton for feeding marine invertebrates. In *Culture of marine invertebrate animals* (Springer), pp. 29–60.
20. Guillard, R.R., and Ryther, J.H. (1962). Studies of marine planktonic diatoms: I. *Cyclotella nana* Husted, and *Detonula confervacea* (Cleve) Gran. *Can. J. Microbiol.* 8, 229–239. <https://doi.org/10.1139/m62-029>.

Cell Reports Physical Science, Volume 4

Supplemental information

**Does the life cycle stage matter
for distinguishing phytoplankton
via fluoro-electrochemical microscopy?**

Jiahao Yu, Minjun Yang, Christopher Batchelor-McAuley, Samuel Barton, Rosalind E.M. Rickaby, Heather A. Bouman, and Richard G. Compton

Contents

Supplemental Figures

Figure S1. Schematic of the vegetative life cycle of *Chlamydomonas*.

Figure S2. Snapshot of supplementary video that showcases three types of *C. concordia* cells under the 20x bright field imaging.

Figure S3. Distribution of the ratio of longest length and its perpendicular width of type 1 (in grey) zoospores and type 3 (in blue) mature cells.

Figure S4. A flowchart indicating the separation protocol of the three types of morphology distinct *C. concordia* cells based on observation and literature reports.

Figure S5. A plot of the measured longest-length and perpendicular width at half cell length. a) zoospores and b) mature cells.

Figure S6. A plot of the cellular projection area measured optically versus that calculated using the measured longest-length and perpendicular width measured at half cell length.

Figure S7. The raw fluorescence intensity of three types of *C. concordia* is plotted against individual radii on a logarithm scale.

Figure S8. The raw fluorescence intensity of three types of *C. concordia* is plotted against the time of 50% fluorescence switch-off (t_{50}) on a logarithm scale.

Figure S9. The number of moles of oxidants delivered to each cell using the characteristic time between the 50% chl-a switch-off and the onset of the catastrophic drop plotted against individual radii on a logarithm scale.

Supplemental Experimental Procedures

Note S1. Separation Protocol and Live Video

Note S2. Raw Intensity Measurements

Supplemental References

Supplemental Figures

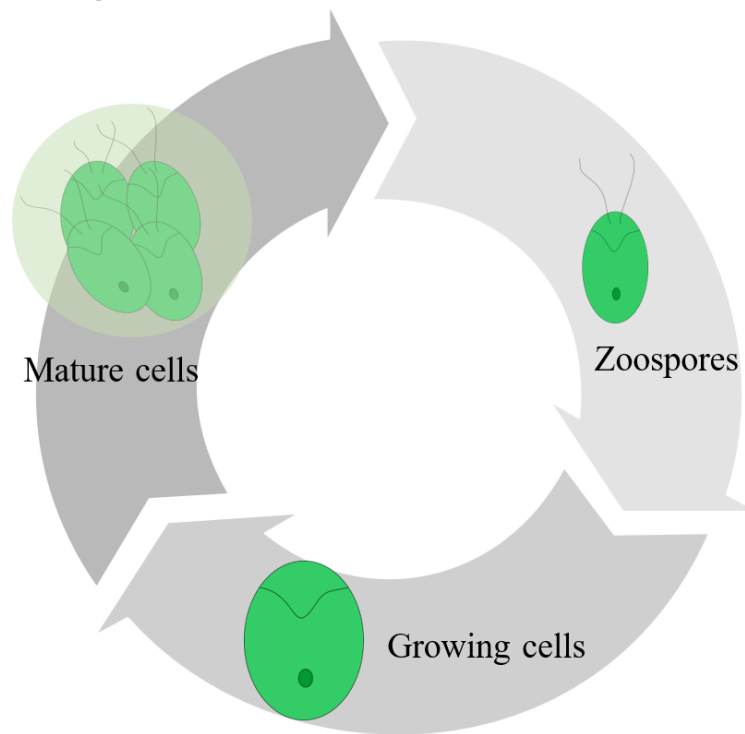


Figure S1. Schematic of the vegetative life cycle of *Chlamydomonas*.

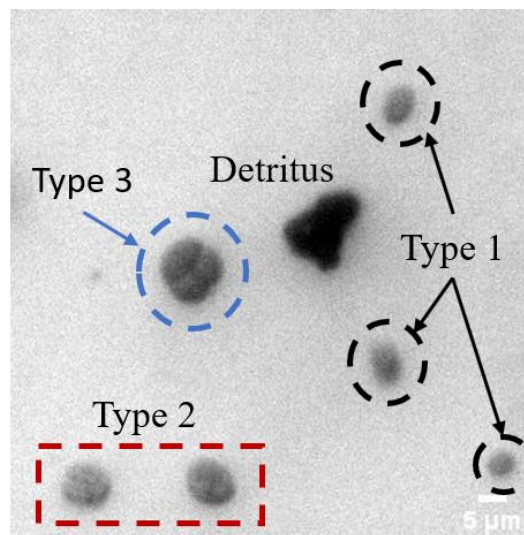


Figure S2. Snapshot of supplementary video that showcases three types of *C. concordia* cells under the 20x bright field imaging.

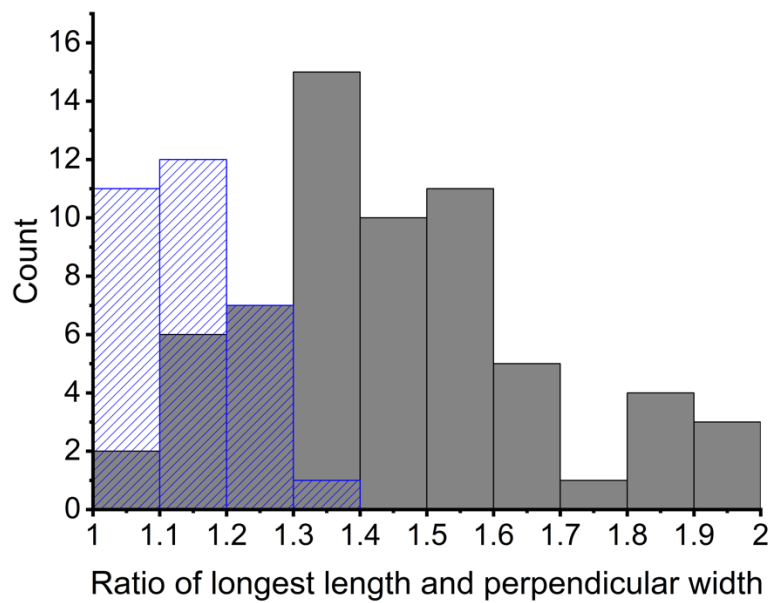


Figure S3. Distribution of the ratio of longest length and its perpendicular width of type 1 (in grey) zoospores and type 3 (in blue) mature cells.

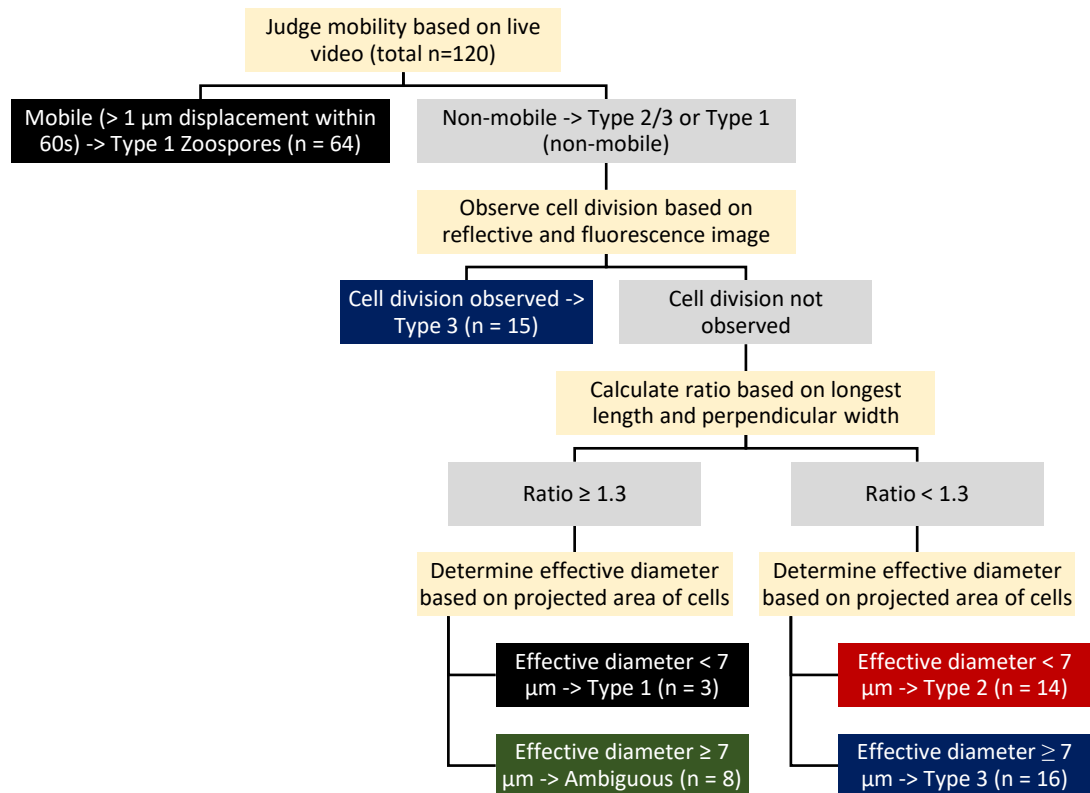


Figure S4. A flowchart indicating the separation protocol of the three types of morphology distinct *C. concordia* cells based on observation and literature reports. Type 1: $n=67$, type 2: $n=14$, type 3: $n=31$ and type 4 (ambiguous): $n=8$.

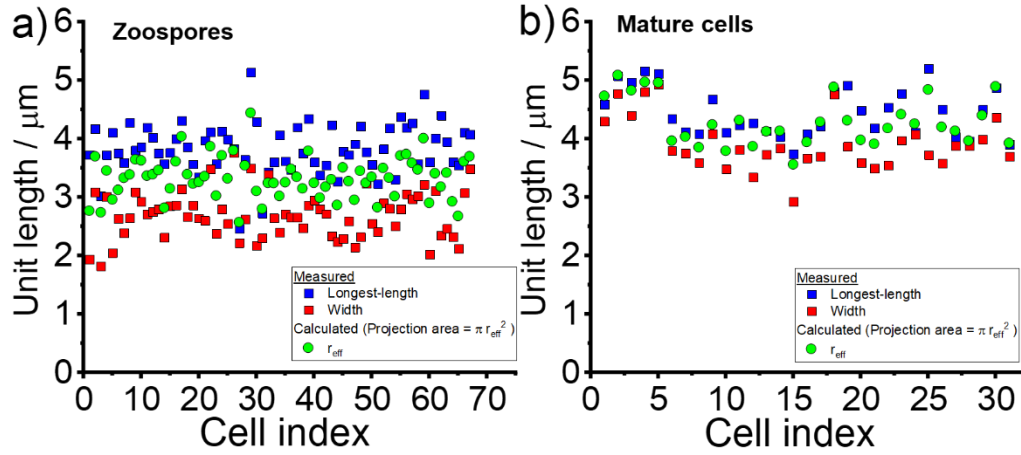


Figure S5. A plot of the measured longest-length and perpendicular width at half cell length. a) zoospores and b) mature cells. Overlaid as green circles is the effective cellular radius of a perfect circle using an equivalent area to that measured optically ($\text{Area} = \pi r_{\text{eff}}^2$).

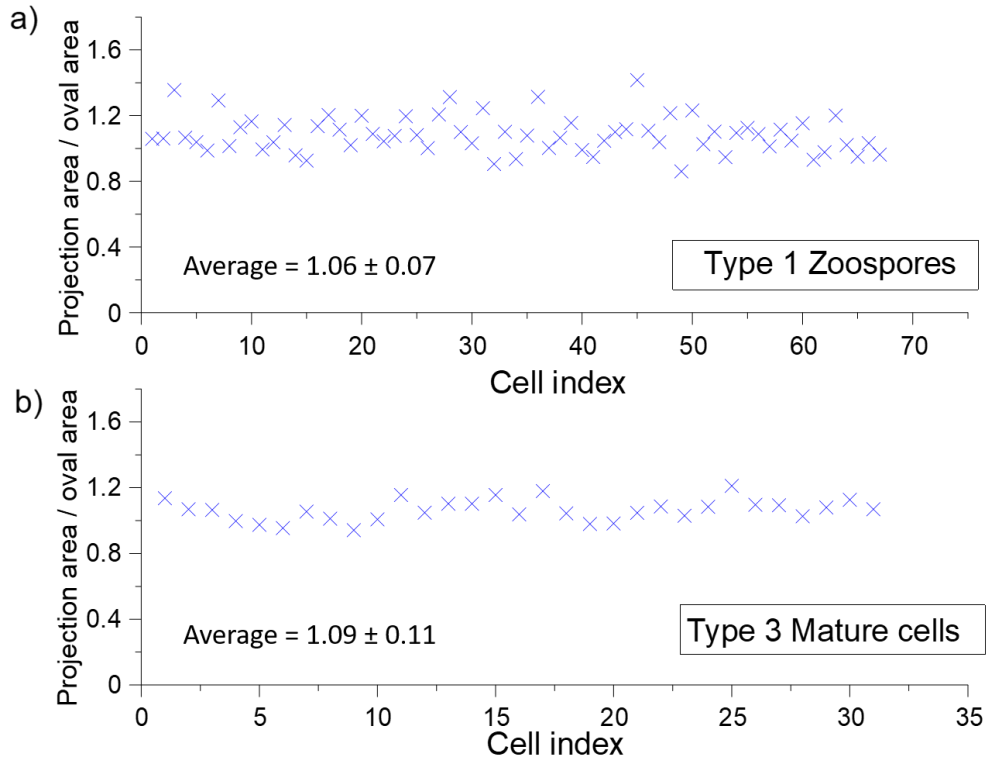


Figure S6. A plot of the cellular projection area measured optically versus that calculated using the measured longest-length and perpendicular width measured at half cell length. a) zoospores and b) mature cells.

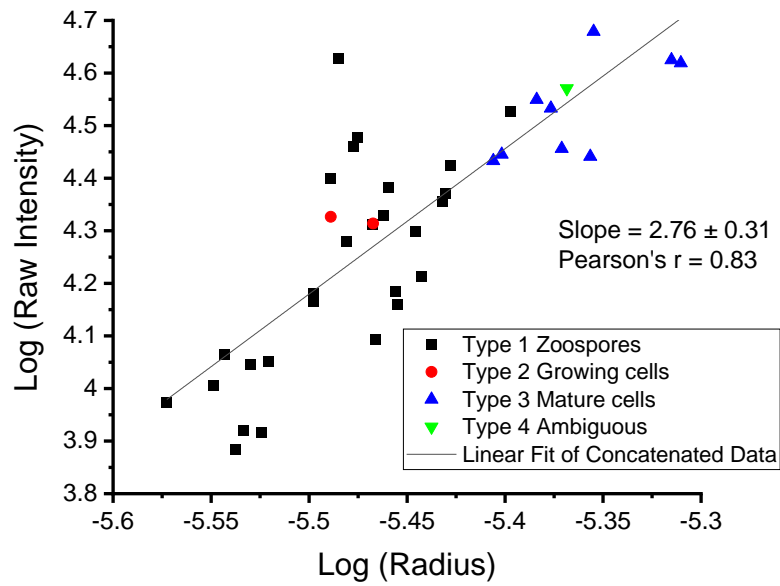


Figure S7. The raw fluorescence intensity of three types of *C. concordia* is plotted against individual radii on a logarithm scale. A slope of 2.76 ± 0.31 is observed.

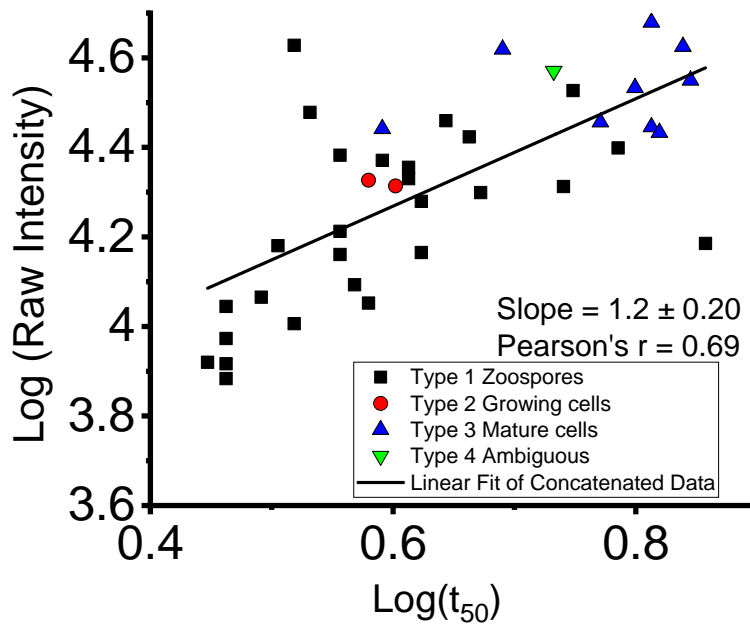


Figure S8. The raw fluorescence intensity of three types of *C. concordia* is plotted against the time of 50% fluorescence switch-off (t_{50}) on a logarithm scale. A slope of 1.2 ± 0.2 is observed.

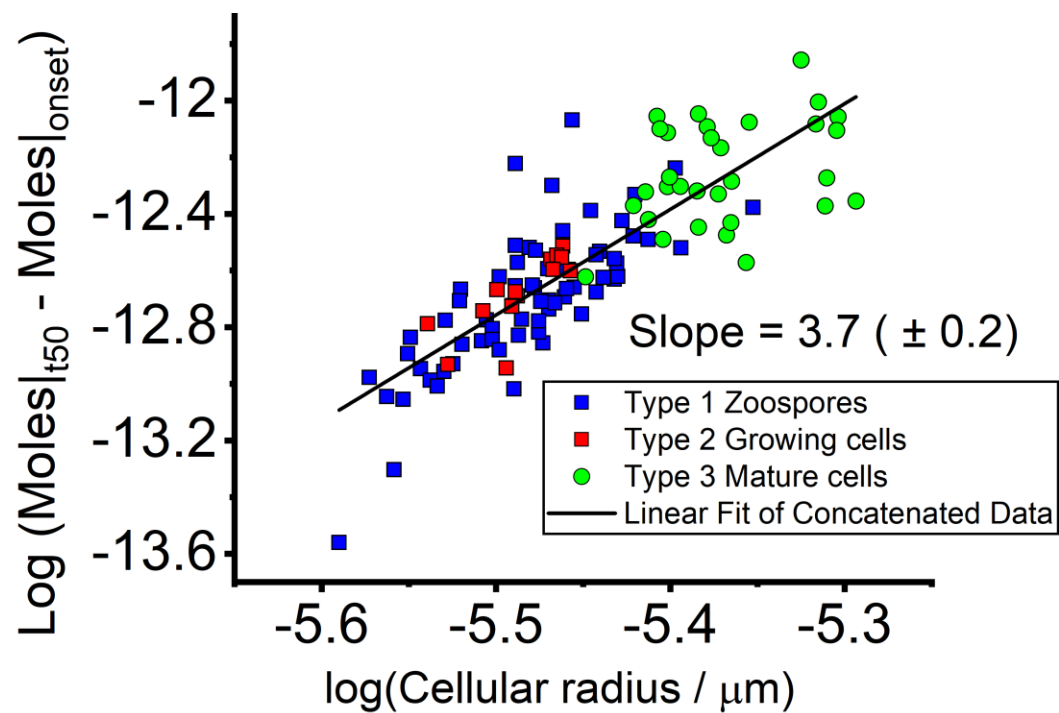


Figure S9. The number of moles of oxidants delivered to each cell using the characteristic time between the 50% chl-a switch-off and the onset of the catastrophic drop plotted against individual radii on a logarithm scale.

Supplemental Experimental Procedures

Note S1. Separation Protocol and Live Video

The life cycles of the *Chlamydomonas* genus have been described in the main text. Figure S1 shows a simple life cycle diagram depicting the life stages of *Chlamydomonas* vegetative cells, fresh water *C. reinhardtii*, which belong to the same genus as *C. concordia* studied in this work. More comprehensive diagrams involving other life cycles in the sexual phase (zygote and gamete) can be found elsewhere in the literature.^{1, 2}

Attached online separately is an experimental video file (Video S1) showing different types of *C. concordia* cells on the surface of the glassy carbon electrode. A snapshot image of the video is shown in Figure S2 where the three different types of cells are annotated as type 1 (zoospores), type 2 (growing cells) and type 3 (mother cells). Note the detritus is foreign and is not associated with the phytoplankton lifecycle as it does not fluoresce. Note that growing cells are in later stages of zoospores within the life cycle where the flagella are retracted prior to transforming into mother cells. Under optical microscopy, and shown in the supporting video file, the flagellated zoospores are either 'free-to-roam' at speeds of $ca\ 10\ \mu\text{m s}^{-1}$ or twitching/pivoting when either one or both the flagellum are stuck to the supporting substrate. This is distinctively different to the lack of flagella of type 2 growing and type 3 mother cells which appear 'stationary' in the timescale of the experiment. Next, some of the mother cells are seen to undergo mitosis to form either 2 or 4 daughter cells which are self-evident under optical imaging (see Figure 1 f). The cellular dimensions of the length: width ratio of zoospores and mother cells, which can be identified via mobility and mitosis, respectively, are measured and plotted as a histogram in Figure S3. As can be seen, cells with a length: width ratio higher than 1.3 can be identified as zoospores. Below a length: width ratio of 1.3, it is either type 3 cells **or** type 2 growing cells which is morphologically intermediate of type 1 and type 3. Lastly, since type 3 is distinctively larger than type 1 or 2, an effective diameter calculated based on projected area is used to further distinguish type 3 from type 2 cells that have a length: width ratio below 1.3. The above observations are summarised as a flowchart in Figure S4 which is used as a separation protocol in the fluoro-electrochemical experiments.

In Figure S3 we showed the ratio of the longest length and perpendicular width of optically identified flagellated zoospores and mature cells. The varying ratio within each cell type is an inherent nature of biological samples as their cellular transition within a life cycle is continuous, non-discrete and most likely out of sync. In the remainder of this section, we provide analysis for, first, the effectiveness of using an effective radius versus the measured longest-length and width of the cell. Second, the deviation from sphericity of zoospores and mature cells by comparing their measured projection area versus the area of a perfect oval calculated using the measured longest-length and width.

Figure S5 shows the effective radius versus the measured longest-length and width of a) zoospores and b) mature cells. The effective radius of each cell was calculated from a perfect circle with an equivalent area to the optically measured projection area. As can be seen, the effective radius is approximately the arithmetic mean of the longest-length and perpendicular width measured at half cell length. This justifies the use of effective radius (or diameter) in the main text to describe the dimension of these near-spherical cells. Figure S6 plots the measured projection area versus that calculated for an oval shape using the measured longest-length and width at the halved cell length. A ratio of $1.09 (\pm 0.11)$ was seen for mature cells and $1.06 (\pm 0.07)$ for zoospores. A generic formula was used to calculate the area of an oval: $\text{area} = \pi * a * b$, where a and b is the major and minor axis. We conclude that, within measurement errors, zoospores are near-perfect oval whereas mature cells are more irregular as evidenced in Figure S2.

Note S2. Raw Intensity Measurements

Figure S7 is a log-log plot of the integrated chl-a fluorescence intensity across each individual *C. concordia* vegetative cell present in a representative fluoro-electrochemical experiment against the measured cellular radius. As can be seen, the slope in the logarithmic scale suggests that the chl-a content within *C. concordia* cells scales with the volume of the cell. Shown in Figure S8 is a log-log plot of the integrated cellular chl-a fluorescence, prior to the

onset of electrochemistry, against the time required for 50% of their fluorescence to be switched off by electrochemical generated oxidants. As can be seen a log-log slope of 1.2 (± 0.2) is seen. This is consistent to the Sand's equation, shown in Equation 1 in the main text, where the total amount of moles of oxidant delivered to each cell is proportional to time raised to the power of 1.5. This suggests a linear relationship between the amount moles of oxidants required to be delivered to the plankton cell against the quantity of chl-a (\propto chl-a intensity).

Supplemental References

- S1. D. P. Weeks and P. S. Collis, *Developmental Biology*, 1979, **69**, 400-407.
- S2. S. Mihara and E. HASE, *Plant and cell physiology*, 1971, **12**, 225-236.